Shock Waves (2009) 19:103–112
DOI 10.1007/s00193-009-0204-z

ORIGINAL ARTICLE

Diffuse holographic interferometric observation of shock wave reflection from a skewed wedge

D. Numata · K. Ohtani · K. Takayama

Received: 1 May 2008 / Accepted: 15 October 2008 / Published online: 12 May 2009

Abstract The pattern of shock wave reflection over a wedge is, in general, either a regular reflection or a Mach reflection, depending on wedge angles, shock wave Mach numbers, and specific heat ratios of gases. However, regular and Mach reflections can coexist, in particular, over a three-dimensional wedge surface, whose inclination angles locally vary normal to the direction of shock propagation. This paper reports a result of diffuse double exposure holographic interferometric observations of shock wave reflections over a skewed wedge surface placed in a 100×180 mm shock tube. The wedge consists of a straight generating line whose local inclination angle varies continuously from 30° to 60°. Painting its surface with fluorescent spray paint and irradiating its surface with a collimated object beam at a time interval of a few microseconds, we succeeded in visualizing three-dimensional shock reflection over the skewed wedge surface. Experiments were performed at shock Mach numbers, 1.55, 2.02, and 2.53 in air. From reconstructed holographic images, we estimated critical transition angles at these shock wave Mach numbers and found that these were very close to those over straight wedges. This is attributable to the flow three-dimensionality.

Communicated by B. Skews and C. Needham.

D. Numata (✉)
Graduate School of Engineering, Department of Aerospace Engineering, Tohoku University, 6-6-01, Aramaki Aza Aoba, Aoba, Sendai 980-8577, Japan
e-mail: numata.daiju@aero.mech.tohoku.ac.jp

K. Ohtani · K. Takayama
Shock Wave Interdisciplinary Application Division, Institute of Fluid Science, Tohoku University, 2-1-1, Katahira, Aoba, Sendai 980-8577, Japan

Keywords Shock wave reflection · Skewed wedge · Holographic interferometry

PACS 47.40.-x · 47.40.Nm · 42.40.Kw

1 Introduction

The reflection of oblique shock waves is one of the fundamental research topics of shock wave dynamics. Regarding two-dimensional shock wave reflections, their patterns are classified, in general, as regular reflection or Mach reflection, depending on shock wave Mach numbers, wedge angles, and ratios of specific heats of test gases. A comprehensive classification of the reflection patterns in unsteady and quasi-stationary flows was given [1]. Ben-Dor [2] recently up-dated shock wave reflection phenomena in unsteady and quasi-stationary flows in the past. However, in previous studies, reflections over two-dimensional wedges were considered. It became a nearly established tradition in shock wave research that shock tube experiments were performed with straight wedges or two-dimensional concave and convex walls [3].

Encouraged by recent advancements in optical flow visualization techniques and fine numerical simulations, we are able to technically discuss various three-dimensional shock wave phenomena. Although two-dimensional flows were easy to experiment and also to analyze, the flows, strictly speaking, accompany more or less three-dimensional features, which were caused by the presence of boundary layers developing along shock tube walls, and intersecting corners of rectangular shock tubes. However, these effects were not usually taken into account. It is necessary to correctly account for these three-dimensional effects. Previous shock wave reflection studies were performed only for two-dimensional models [3] and very rarely for three-dimensional cases.

Critical transition angles of shock wave reflections over cones, whose configurations differ significantly from wedge shapes but two-dimensional analytical approaches are still valid, are more or less close to those over wedges [4,5].

Recently, the delayed transition from regular to Mach reflection was found to appear even in the shock wave reflection over cones [6]. This was caused by the presence of boundary layers developing from the apex of cone. The boundary layer displacement thickness locally increased the cone's nominal apex angle and hence created regular reflection at the cone apex angle at which Mach reflection should take place. Watanabe and Takayama [7] visualized the reflection of a blast wave from a tilted cone. A planar shock wave of Mach number 1.2 was discharged from the end of a 230 mm diameter shock tube into open air and impinged immediately on a cone of apex angle 70° which was tilted by 25° from the shock tube axis. Hence, the shock impingement angle on the cone surface varied locally from 45° to 95°. The resulting shock wave reflection pattern varied from Mach reflection to regular reflection depending on the local intersecting angle. With double exposure holographic interferometry, they observed the reflected shock transition from regular to Mach reflection over the tilted cone.

Timofeev et al. [8] numerically studied the reflection of planar shock waves over a 30° swept back cylinder placed on a shock tube bottom wall and successfully visualized, by using diffuse double exposure holographic interferometry and adopting the time interval of double exposures at a few microsecond, the spot on the cylinder at which reflected shock wave pattern changed from regular to Mach reflection.

As an extension of our continuous quest for shock wave reflections over a swept back cylinder and an inclined cone, we constructed a skewed wedge, which consisted of straight oblique generating lines varying continuously from 30° to 60°. Unlike the tilted cylinder or the inclined cone, the present skewed wedge has a relatively simple configuration. We then expected that the shock wave reflection over it, in principle, would be an extension of shock wave reflection over wedges and that regular and Mach reflections should co-exist somewhere on its surface.

We installed it in a 100×180 mm shock tube and visualized with diffuse double exposure holographic interferometry. In observing reconstructed holographic images with the naked eye, we could clearly recognize the co-existence of regular and Mach reflections. However, diffuse holographic images, being three-dimensional, are not necessarily as clear as that viewed with naked eyes but we managed to record them in a two-dimensional plane. Recorded images were just clear enough to estimate the location of reflected shock transition angles. The shock Mach numbers tested were 1.55, 2.02, and 2.53 in air. The slight discrepancy from the prediction based on the two-shock theory [2] was found, which would show three-dimensional effects.

Table 1 Test conditions

	Ms	*Re*	Test gas (kPa)	Driver gas (kPa)	Δt (μs)
Case 1	1.55	2.6×10^5	Air (10)	N_2 (50)	3
Case 2	2.02	5.2×10^5	Air (10)	He (50)	3
Case 3	2.53	7.7×10^5	Air (10)	He (300)	2

2 Experiments

2.1 Shock tube

Experiments were performed in a diaphragm-less 100 × 180 mm shock tube at the Interdisciplinary Shock Wave Research Laboratory (ISWRL) of the Institute of Fluid Science, Tohoku University. This shock tube was originally constructed for basic data acquisition supporting the Apollo Project in the 1960s at the Institute for Aerospace Studies of University of Toronto (UTIAS) and donated to the ISWRL in 1994 as a symbol of mutual research collaboration. We refurbished it by elongating its original high-pressure chamber of 2.5 m in length and 150 mm in inner diameter to 5 m in length and 155 mm in inner diameter one by replacing its original diaphragm section with a diaphragm-less operating system. We eventually improved the degree of shock tube repeatability in terms of scatter of shock wave Mach numbers to be ±0.3% for shock wave Mach numbers from 1.5 to 5.0 in air. We constructed a new test section with a view field of 180 × 1,100 mm made of stainless steel, thus we would be able to observe a full length of shock tube flows at higher shock Mach number (for details see [9]). The test gas was air at room temperature and the driver gas was helium. Table 1 summarizes the test conditions.

Reynolds numbers *Re* in Table 1 are defined by a shock tube width of 100 mm as a characteristic length and the conditions behind the incident shock waves. Δt designates the time interval between the first and second exposures.

2.2 Wedge model

Figure 1a shows the skewed wedge model which is 100 mm in width, 70 mm in length, and 110 mm in height. Its shape is analytically given by (1). The surface consists of straight generating lines which are oblique to the direction of the shock tube axis, linearly varying from 30° in the near side to 60° in the far side. The shape is skewed similar to a plow surface.

The shape is three-dimensional. We, at first, believed that it was too complex to be manufactured with an ordinary milling machine. However, it was readily manufactured with a numerically controlled milling machine. Its shape is written

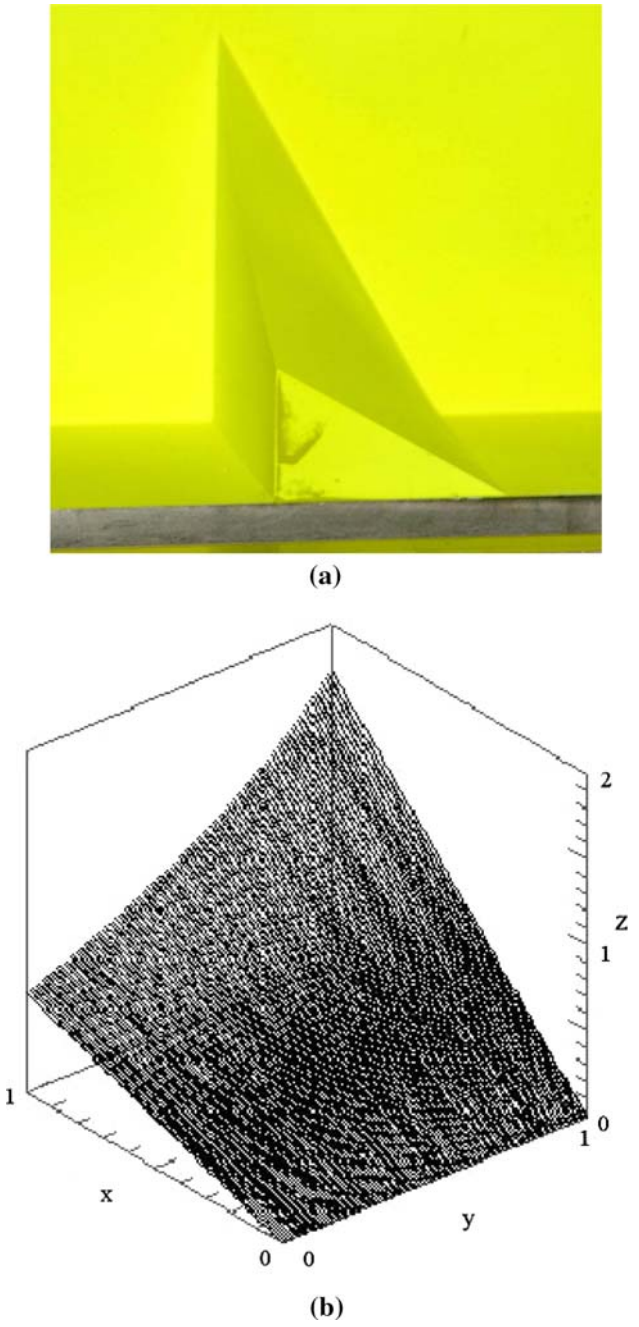

Fig. 1 Skewed wedge model: **a** photograph; and **b** graphic display described by (1)

in x, y, z coordinates as

$$z = x \tan (1 + y/L)\pi/6, \tag{1}$$

where L is the width of 100 mm. Its surface was mirror polished by hand.

2.3 Visualization

Figure 2 shows the present holographic arrangement. The light source was a double pulse ruby laser, LUMONICS

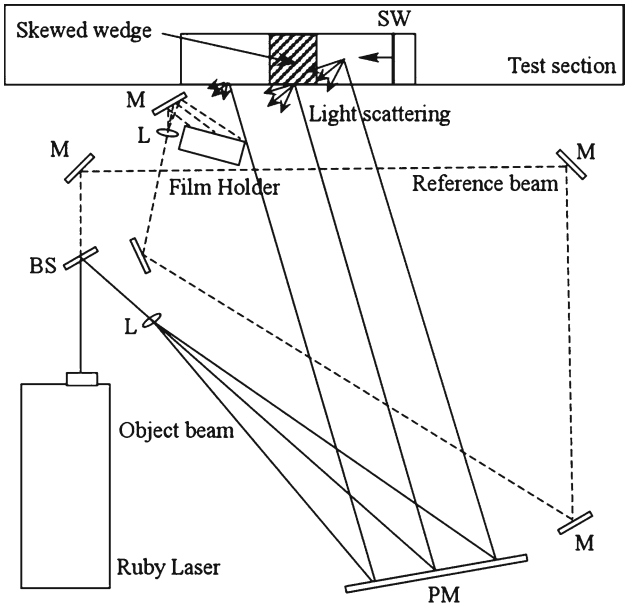

Fig. 2 Optical setup of diffuse holographic interferometry

HLS3 with a pulse duration of 25 ns, 1J per pulse at TEM_{00} mode, and wave length of 694.3 nm. A source laser beam was split into object and reference beams with a 60:40 beam splitter. Then 60% of the source laser beam intensity was reflected from a 500 mm diameter Schlieren mirror, which collimated the object beam and uniformly illuminated the test section.

This optical setup is, in principle, similar to that in [9]. Holographic information randomly reflected from the test section was transmitted onto a 100 × 125 mm AGFA 10E75 sheet film which was placed to obliquely face the test section. About 40% of the source laser beam intensity was transmitted by the reference beam and eventually superimposed with the object beam on the holographic film.

To achieve diffuse reflections of the object beam, we replaced a test section window on the far side with a stainless steel plate and coated its surface with yellow fluorescent spray paint. We also spray painted the shock tube upper and lower walls, and the skewed wedge surface as uniformly as possible, and illuminated it with the 500 mm diameter collimated object beam. The spray paint has a high reflectivity to the ruby laser wavelength and hence the object beam was reflected very efficiently from the wall surfaces. Spray paint coated surfaces were very slightly roughened and its surface roughness was equivalent to that of #2000 sandpaper, which produces surface roughness of 2,000 sand grains per 24.5 mm in other words, surface roughness of about 10 μm. This surface finish cannot be compared to a mirror surface finish but would not significantly affect the shock wave motion [10].

Spray paint coated surfaces reflect the collimated object beam randomly. Then the reflected beams were modulated by density variations in the test section during the double

exposures and transmitted the phase information onto a holographic film, which was facing the test section. We placed the film in an optimized position and orientation by trial and error and believe that we collected holographic information most efficiently under the present experimental conditions.

This was not conventional image holography. We were unable use an image focus lens. Thus the image's spatial resolution could not be as sharp as with image holograms. It simply depends on the size of holographic film used to collect the holographic information. In the present experiments, we could place a 100 × 125 mm holographic film facing the test section as seen in Fig. 2.

Distributing pressure transducers, Kistler model603B, along the shock tube, we detected the arrival of the incident shock wave and estimated the shock wave velocity. One of the pressure transducer's output signals was used to trigger the Q-switch ruby laser. To distinctively record shock wave shapes, we performed double exposures at a short time interval Δt, as tabulated in Table 1. It was 2 μs for $Ms = 2.53$; and 3 μs for $Ms = 1.55$ and 2.02.

Phase change which happened to occur during these time intervals was recorded on a holographic film and was extracted only through the process of reconstruction. The distance for a shock wave to travel in such a short time interval can be about 1.2 mm, which is equivalent to a displacement of 0.4 mm on a reconstructed holographic image at a magnification ratio of approximately 0.3. Shapes of shock waves were recorded as sharp discontinuous curves. This arrangement was already used by Meguro [11] who succeeded in visualizing three-dimensional shock waves reflected from the corner of two perpendicularly intersecting straight wedges. It was also used by Timofeev et al. [8] who visualized three-dimensional shock wave reflections over a swept back cylinder.

We reconstructed holograms by illuminating them with a 200 mm diameter collimated Argon-ion laser beam by using a similar optical arrangement as with the construction of holograms. Then a real image of shock wave reflection over the skewed wedge surface was observable. The resulting three-dimensional shock wave images were clearly seen with the naked eye. We reconstructed holograms from various view angles by using a digital reflex camera attached with a zoom lens, Nikon AF Micro NIKKOR 60 mm 1:2.8.

However, to our disappointment, the resulting images recorded on a film plane were not as sharp as those in image holograms. As a future task, we will try to record three-dimensional holographic images from view angles of every 5° and then restructure these collected images numerically in a three-dimensional display.

2.4 Soot film observation

Slip lines emerging from a triple point would become vortices on the wedge surface and exhibit shear forces, which locally scratch the wedge surface. In detonation studies, cell structures consisting of a slip line and three shock confluence is observed, which is, in principle, a Mach reflection. The presence of the cell structures is well identified as diamond patterns on sooted plates placed in detonation tubes. Likewise, we used the sooted plate technique over the skewed wedge surface to identify the presence of Mach reflection. We exposed the wedge to a kerosene flame and uniformly blackened it. Slip lines developing from the triple points would become vortex sheets and would remove soot particles from the blackened wedge surface. Figure 3 shows the wedge surface coated with kerosene smoke.

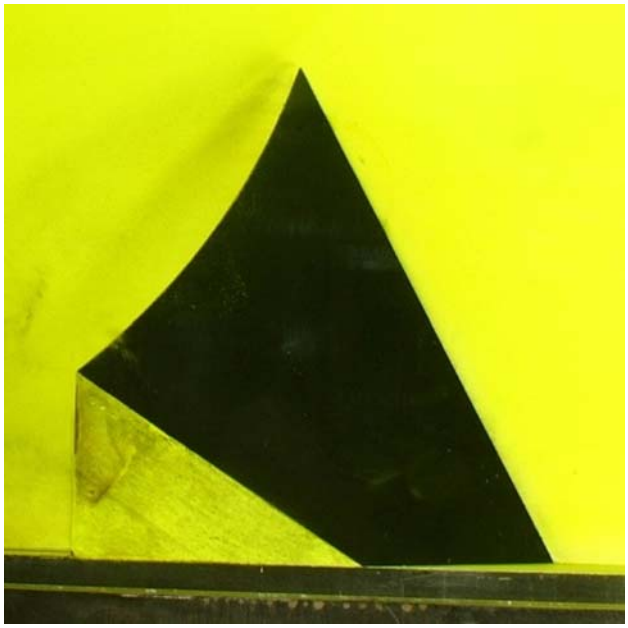

Fig. 3 A kerosene soot blackened wedge surface

3 Results and discussion

3.1 Reconstructed images

We performed ten experiments for case 1 with a nominal shock wave Mach number of $Ms = 1.55$, and obtained six distinctive Mach reflections that are clear enough to identify the critical transition angle. On the frontal wedge surface of 30°, we could clearly see a Mach reflection pattern and the presence of its triple point. With the increase in the wedge angle toward the far side, the triple point position moved and then disappeared. We then defined the critical transition angle as the wedge angle at which the triple point disappeared. Unlike straight wedges, inclination angles vary with the distance from the side wall, the critical transition angle from the three dimensional images was not determined as accurately as with straight wedges.

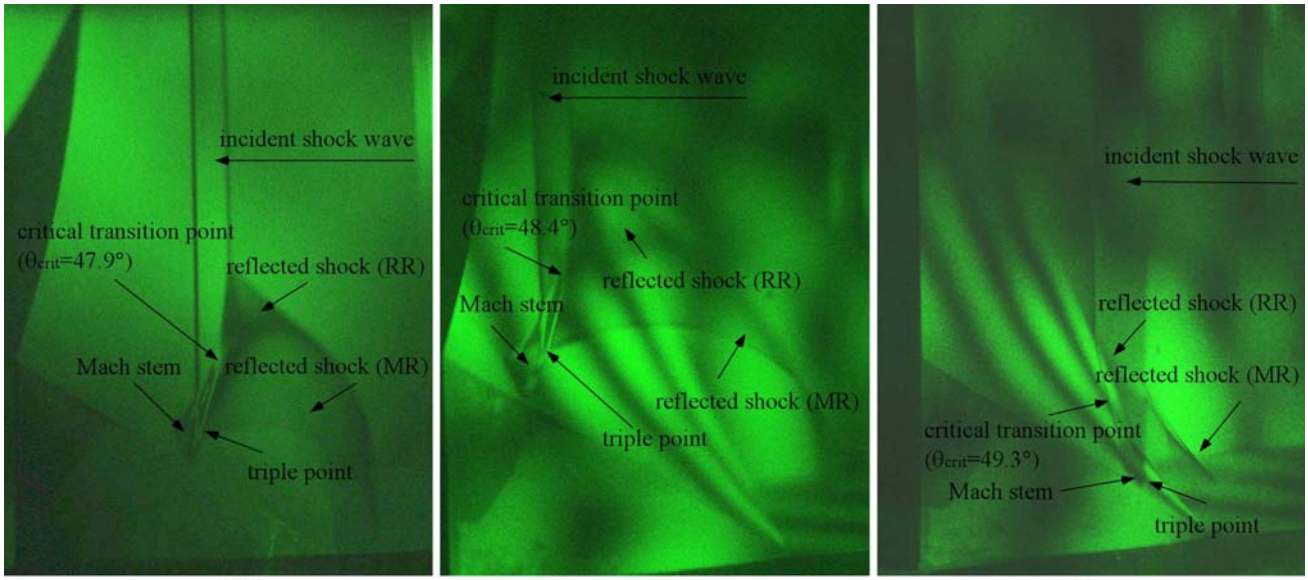

Fig. 4 Reconstructed images for $Ms = 1.55$: **a** 47.9°; **b** 48.4°; and **c** 49.3°

Table 2 Summary of experiments

Shot no.	θ_{crit} (degree)	Ms
06050310	50.77	2.54
06050401	51.32	2.54
06050404	50.58	2.53
06050406	51.94	2.53
06050408	50.68	2.53
06050410	50.74	2.53
06051302	49.90	2.00
06051303	50.38	2.00
06051401	50.15	2.02
06051405	49.72	2.02
06051503	50.00	2.04
06051506	49.99	2.02
06051509	50.02	2.02
06050307	48.43	1.53
06050308	49.31	1.55
06050417	47.96	1.53
06053105	48.60	1.55
06053106	49.04	1.55
06060101	47.97	1.55

Figure 4a–c shows reconstructed images of $Ms = 1.55$ as tabulated in Table 2. Three-dimensional images displayed in a two-dimension plane are not necessarily sharp but wave patterns can be recognized. In Fig. 4, typical wave patterns are explained. We can identify, at least, a shape of a single Mach reflection on a 30° wedge and vaguely recognize a regular reflection pattern on a 60° wedge. The Mach stem visible on the shallow wedge started to shrink toward the steep wedge surface and disappeared in the middle of the wedge. Then the spot at which the Mach stem disappears is identified. From the spot position in the Y-axis in Fig. 1b, we can readily determine the critical transition angle. We have an uncertainty of about 1.5 mm which is equivalent to about ±0.5° in determining angles. So far as examining reconstructed images in Fig. 4a–c, the critical transition angles scattered from 47.9° to 49.3°. The transition angles increase slightly with the increase in distance from the leading edge.

We drew shock polar diagrams for wedge angles at every 5° from 30° to 60° and superimposed them in a pressure-deflection angle plane. An incident shock polar I is drawn at a given wedge angle and a shock wave Mach number of $Ms = 1.55$. A reflected shock polar R is drawn from the given value of pressure on the I-polar [2]. Figure 5 shows a family of shock polars for $Ms = 1.55$. I-polar and R-polar combinations are drawn every 5° from 30° to 60°. Intersection points of individual I- and R-polar combinations on the right hand side of the I-polar indicate the flow deflection angle θ and the normalized pressure behind the Mach stem and reflected shock wave. Drawing I- and R-polars with increasing wedge angles, we can determine the shock wave over-pressure behind the Mach stem on the wedge surface.

Figure 6a–c shows reconstructed images for $Ms = 2.02$ as tabulated in Table 2. We examined seven images out of fifteen experiments. Figure 6c shows a typical transitional Mach reflection [2]. We can see a kink in the reflected shock wave. A typical transitional Mach reflection on the shallow wedge and a regular reflection on the steep wedge are clearly

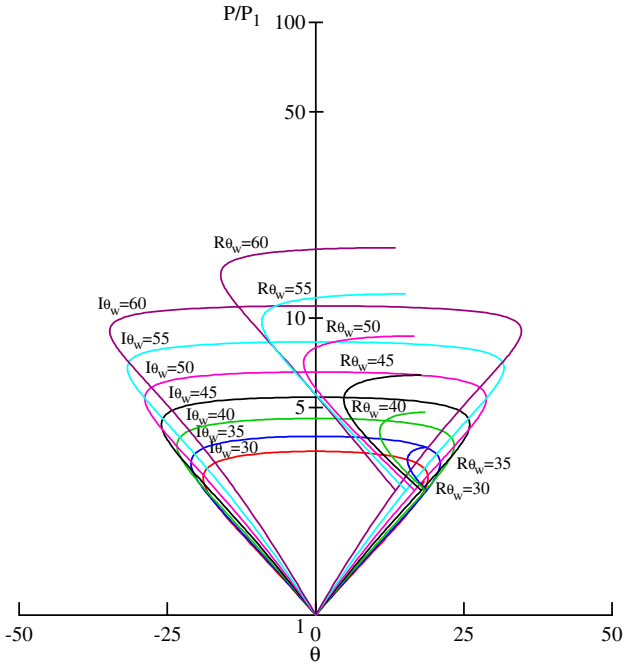

Fig. 5 Shock polar for $Ms = 1.55$

observed. In each photo in Fig. 6, the Mach stem disappears at a critical transition point between 30° and 60° wedges. Then we can identify how the critical transition angles vary slightly in Fig. 6, depending on the distance from the leading edge. So far we estimated from Fig. 6a–c, that it ranged from 49.7° to 50.3°. Broad fringes visible in Fig. 6b, c had no physical significance and were attributable to uncontrolled modes of source laser light. Figure 7 shows a family of shock polars.

Figure 8a–c shows reconstructed images of $Ms = 2.53$ as tabulated in Table 2 and six images were examined out of ten experiments. Figure 8c shows a typical double Mach reflection pattern [2]. We can see the first and a second triple points and the corresponding first and second slip lines on a shallow wedge and a regular reflection on the steep wedge. A Mach stem emerging from the first triple point disappears at a spot between 30° and 60° wedges. We could estimate the corresponding critical transition angles in Fig. 8a–c. The critical transition angle increased with the position of observation from the leading edge. It ranged from 50.6° to 51.9°. Figure 9 shows a family of shock polar for $Ms = 2.53$.

Figure 10 summarizes the results of shock polar diagrams and pressure variations behind the Mach stem or reflected shock waves vs. wedge angles at $Ms = 1.55$, 2.02 and 2.53. The ordinate designates pressure normalized by the initial pressure and the abscissa designates wedge angle. The pressures monotonically increase with wedge angles with a discontinuity at the critical transition angle. The Mach reflection and regular reflection co-exist over the present skewed wedge surface. The pressure behind the Mach stem on the shallower wedge is lower than that behind reflected shock waves on a steeper wedge.

Hence the particle flows are not necessarily directed along the generating lines of the wedge surface but would be slightly deflected obliquely from steeper side to shallower side. In short, the particle flow slides along the wedge surface. If we assume a control plane locally along the direction of the deflected particle flow, that is, slightly oblique to the shock tube axis, the nominal critical transition angle would be larger than that predicted by two-dimensional transition. However, this assumption is a kind of instinctive interpretation. The

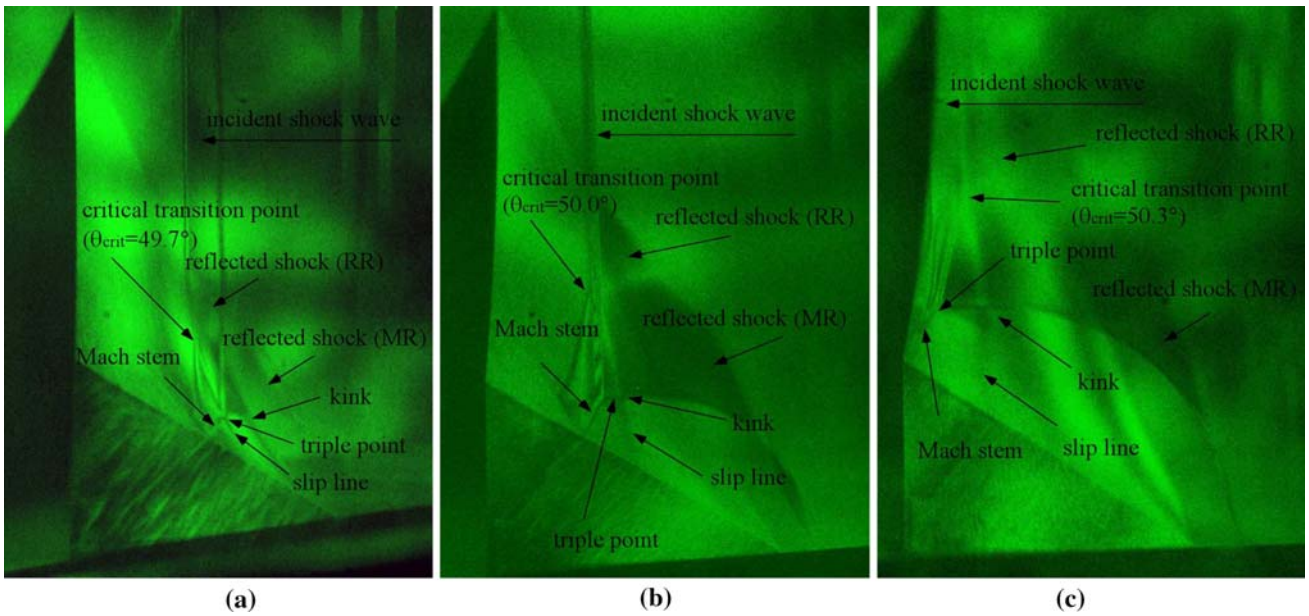

Fig. 6 Reconstructed images for $Ms = 2.02$: **a** 49.7°; **b** 50.0°; and **c** 50.3°

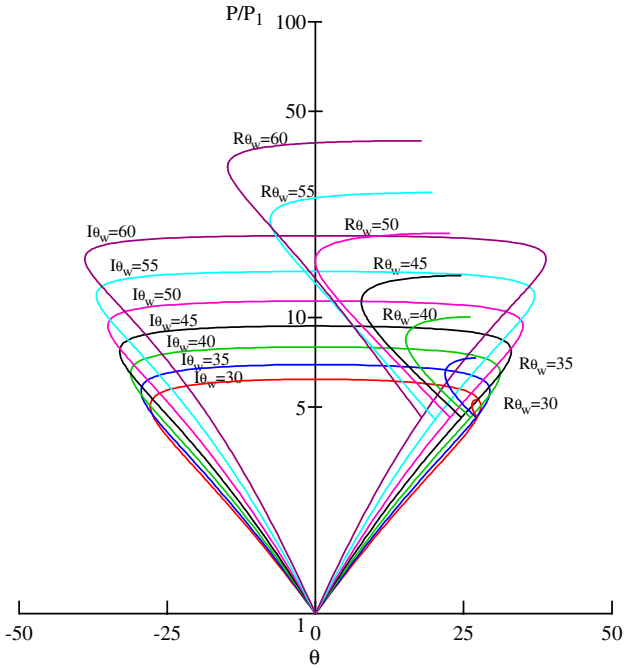

Fig. 7 Shock polar for $Ms = 2.02$

particle flow deflection would vary with the distance from the leading edge along which the incident shock moved. Hence, the critical transition angle would also vary with the distance from the leading edge. We can speculate that, as an extreme case, in the vicinity of the leading edge the reflection pattern should be independent of the side flow and only affected by the presence of a wall boundary layer. It would be predicted by a two-dimensional model. When the incident shock wave moves reasonably away from the leading edge, the three-dimensionality would be prominent. Within the transient distance, the critical transition angle would vary with the distance from the leading edge. Within the resolution of the present data evaluation, the critical transition angles estimated in Figs. 4, 6, and 8 increased slightly with the distance form the leading edge.

We may test with a skewed wedge whose angles between the two sides are greater than the present case, the deviation of critical transition angles from two-dimensional prediction would be larger.

It should be noticed that, in addition to the three-dimensionality of the model, the presence of the wall boundary would also contribute to the reflected shock transition. Regular reflection took place in the vicinity of a wedge's edge even when the wedge angle warranted Mach reflection. Then the transition to Mach reflection indeed was delayed [12] and the delayed transition to Mach reflection varied with the initial pressures. It is caused by the effect of the boundary layer displacement thickness developing from the wedge's leading edge, which has the effect of an increased wedge angle.

Likewise we have to consider, in addition to the presence of the side flow, the contribution of wall boundary layers to the reflected shock transition over the skewed wedge. However, at this stage, we would like to limit our discussion within the resolution of our achievable data evaluation.

Figure 11 shows a summary of the present experiment: a comparison of the experimental critical transition angles with predictions based on two-shock theory [2]. The ordinate

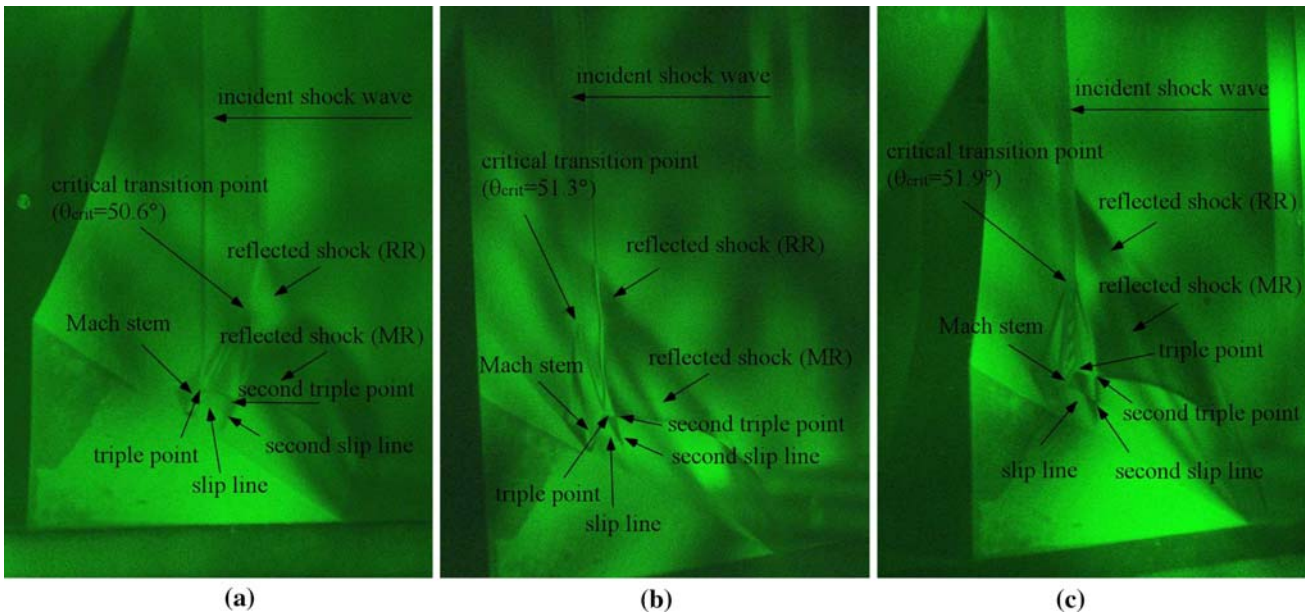

Fig. 8 Reconstructed images for $Ms = 2.53$: **a** 50.6°; **b** 51.3°; and **c** 51.9°

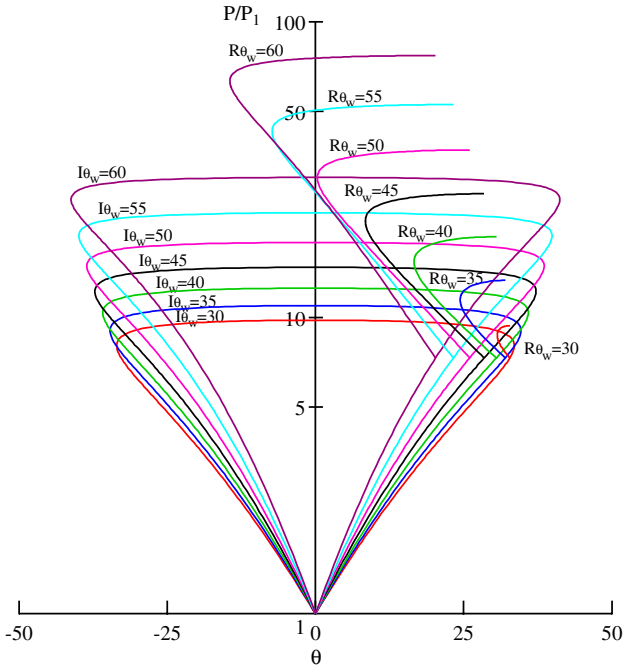

Fig. 9 Shock polar for $Ms = 2.53$

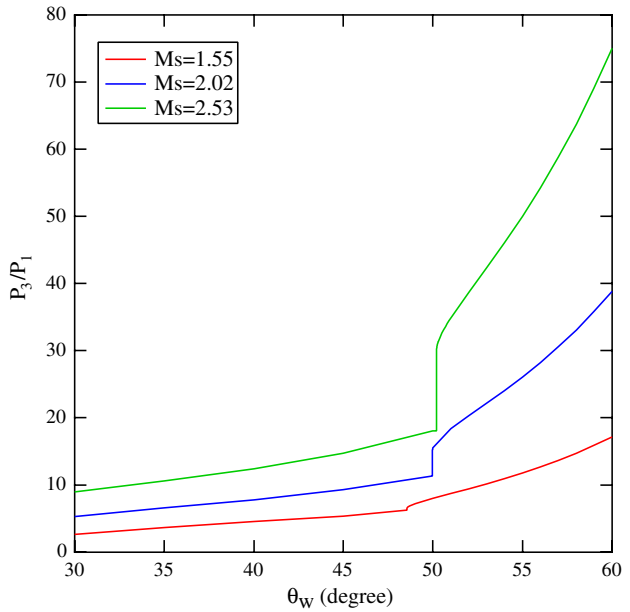

Fig. 10 Over-pressures behind Mach stem and reflected shock against wedge angles

designates the critical transition angle θ_{crit} and abscissa designates shock wave Mach numbers *Ms* in air. The solid line shows the prediction using two-shock theory, filled circles designate the present experimental results, open circles show critical transition angle for wedge results, Smith [13], open triangles and filled triangles show cone results of [4,5], respectively. Just for reference, we compared wedge results with those over cones.

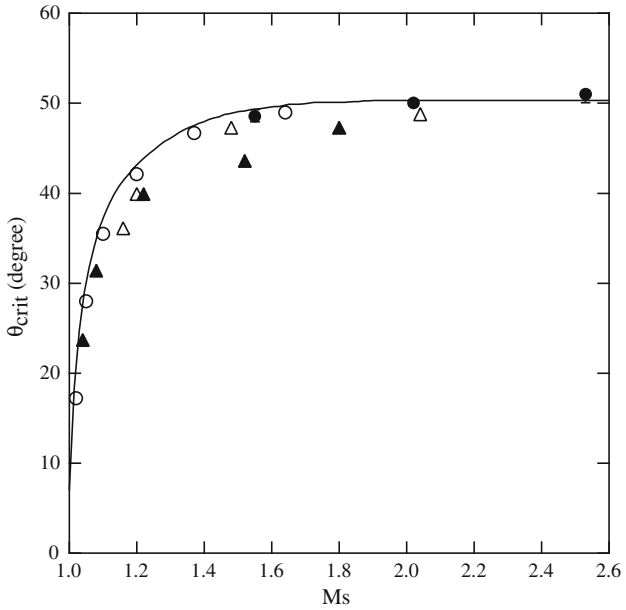

Fig. 11 Comparison between θ_{crit} and *Ms*: *Filled circles* designate the present results; *open circles* plane wedges [13]: *filled and open triangles* show cone cases [4,5], respectively

The cone results do not differ significantly from the wedge results. Unlike two-dimensional reflections over straight wedges, the present results over the skewed wedge are scattered slightly but are closer to the prediction. As seen in Figs. 4, 6, and 8, the trend of scatter is consistent indicating the flow three-dimensionality, typically the presence of side flows. However, it should be mentioned that contributions of side flows and wall boundary layers to reflected shock transition should be discussed in the future when we improve the resolution of visualization. To assure the contribution of surface roughness on critical transition angles, the reflected shock transition over plane wedges with saw tooth shaped surface roughness [10] and roughened concave wedges using sand paper were observed [14]. The critical transition angles over roughened wedge surfaces are usually smaller than those over smooth wedge surfaces, because the boundary layer displacement thickness increases the apparent wedge angles behind the reflected shock wave. Hence, the present consistent but slight shift of critical transition angles would be a result of side flows being canceled out by surface roughness effects.

3.2 Soot surface record

To identify the effect of vortex sheets sweeping over the skewed wedge surface, we tried to observe the passage of shock waves over a soot coated wedge surface. Initially we wanted to observe dynamic soot particle removal from the skewed wedge surface by high speed video recording at a

framing rate of one million frames per second. The dynamic image resolution was so poor that we failed to identify the process of soot particle removal from the sooted wedge surface. We then decided to examine a sooted wedge surface on which the shock wave passed. We found eventually that soot particles were relatively well removed only in the case of $Ms = 2.53$ but in other weaker shock cases soot particles remained and were hardly removed. In $Ms = 2.53$ the resulting shear forces were intense enough to effectively remove soot particles. The intensity of the shear force or vortex is proportional to the magnitude of pressure behind the reflected shock wave as shown in Fig. 10 and enough to scratch the soot wedge surface.

Figure 12a shows a photograph of a soot coated wedge surface exposed to a $Ms = 2.53$ shock wave. Grey and white regions represent soot coated and soot free regions, respectively. The soot free region is clearly distinguished from the soot coated region. Along the boundary between these regions a relatively broad black stripe is observed. To identify the region and boundary of the soot free region, we marked, using computer aided image processing, the skewed wedge surface with lines every 6° and a normalized distance interval of 0.2.

Figure 12b is a sketch of Fig. 12a obtained by image processing. The ordinate designates the wedge angle and the abscissa designates the normalized distance from the leading edge. The red curve indicates the boundary between the soot free region and sooted region. Filled circles with error bars show the critical transition points as summarized in Table 2. A black stripe in the central part of Fig. 12a is a soot attached region displayed by a dark blue curve in Fig. 12b. A purple line indicates the predicted critical transition angle based on the two-shock theory [2].

Within the scatter of the data points, the critical transition angles increase slightly with the distance from the leading edge. The boundary of the soot free region spreads for the entire leading edge and quickly moves to about 44° at a dimension-less distance of 0.2 and gradually increases to the trailing edge, at which the soot free region started to spread. The reflected shock wave from the path of the triple point of Mach reflection on the shallower wedge and that from the reflected shock wave of regular reflection at steep wedge angles merges with the reflected shock wave at the leading edge. These shock wave patterns are clearly observed in the reconstructions of holograms as seen in Figs. 4, 6, and 8.

At $Ms = 2.53$, the local flow is supersonic and hence at the leading edge, reflected shock waves are detached over the steeper wedge and attached over the shallower wedge. This might have affected the formation mechanism of soot particle free region at the leading edge area. However, it is, in principle, caused by the presence of a vortex recirculating at the compression corner between the wedge and shock tube bottom wall. The soot free region at the trailing edge is formed

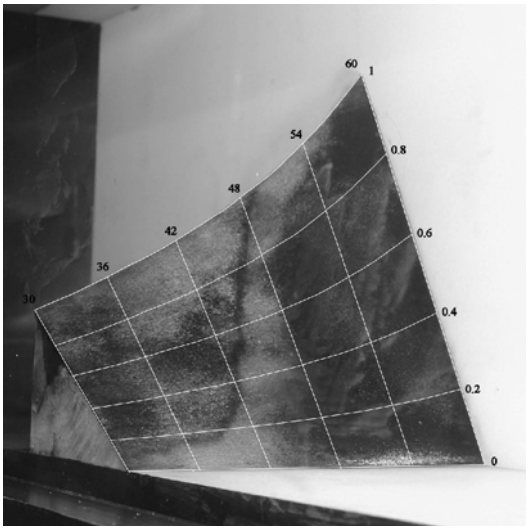

(a)

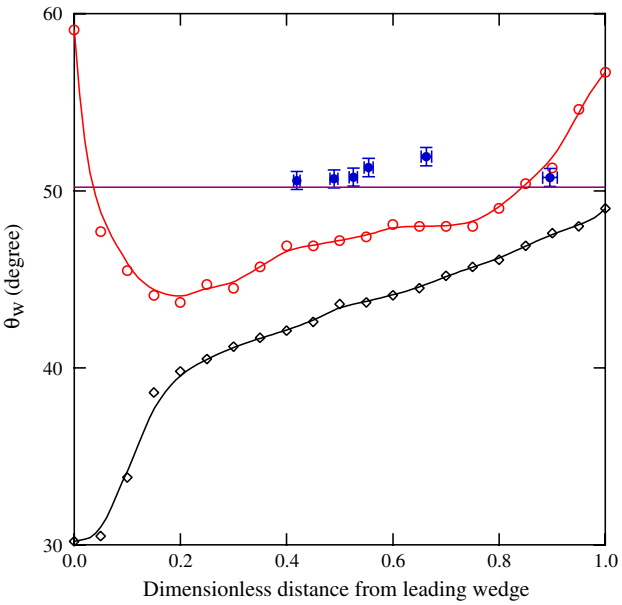

(b)

Fig. 12 Soot surface record: **a** Result for $Ms = 2.53$; and **b** sketch

due to the flow turning at the backward facing corner. In high speed video recording, we observed the consistent release of soot particles at the trailing edge upon shock passage over the wedge. This would have created the entire soot free region at the trailing edge. In conclusion the soot free regions at the leading and trailing edges are not caused by the mechanisms of reflected shock transition.

The soot free region is, in principle, created by the removal of soot particles from the wedge surface. The present soot free region is similarly observed when a detonation wave passes over a soot coated surface. It is believed that the sooted surface is scratched by the passage of cellular structures behind detonation fronts, which are vortices emerging from the triple

point. This mechanism is historically well understood as the formation of Mach-V as documented by Reichenbach [15].

Points of initiation of transition are shown in filled circles in Fig. 12b, whose transition angles slightly deviate from the boundary of the soot free region consistently by approximately 5° between dimension-less distances of 0.4 and 0.7. Such a departure of the soot free region would indicate the presence of a transition time for slip lines to develop in a vortex intense enough to roll up soot particles.

The appearance of a broad soot line remaining in the soot free region cannot be explained. In order to interpret this broad soot line we are planning to perform a three-dimensional numerical simulation.

4 Conclusions

As a part of the continued studies of three-dimensional shock wave reflection, we visualized, by using diffuse holographic interferometry, reflections of shock waves from a skewed wedge surface on which the wedge angle varies continuously from 30° to 60°. Results obtained are summarized as follows:

1. We succeeded in applying double exposure diffuse holographic interferometry with relatively short time intervals to visualize, with reasonably good spatial resolution, three-dimensional reflected shock waves on a skewed wedge surface. From the extrapolation of the resulting reconstructed images, we could estimate the point of Mach stem termination on the wedge surface.
2. The critical transition angle was not uniquely constant for a given shock wave Mach number and varied only very slightly with increasing distance from the leading edge of the wedge. This is attributable to pressure increases behind the Mach stem or reflected shock wave with wedge angle, representing a weak three-dimensionality.
3. The critical transition angles, even though slightly variable, are very close to the values predicted by two-shock theory. In the near future, a three-dimensional numerical simulation should be carried out in order to compare the present image data.

We would like to encourage those who are interested in numerical simulation of the present experiments and upon requests are able to offer image data listed in Table 2. The image data listed in Table 2 is also available in the ISWI Archive which is open to all the International Shock Wave Institute members.

Acknowledgments The authors would like to express their appreciation to Mr. S. Hayasaka of the Interdisciplinary Shock Wave Research Laboratory (ISWRL) of the Institute of Fluid Science, Tohoku University for his collaboration throughout the present experiments. This project was in part supported by the Grant-in-Aid for Scientific Research 12CE2003 offered by the Ministry of Education, Culture, Sport, Science and Technology, Japan.

References

1. Ben-Dor, G., Takayama, K.: The phenomena of shock wave reflection—a review of unsolved problems and future research needs. Shock Waves **2**, 211–223 (1992)
2. Ben-Dor, G.: Shock Wave Reflection Phenomena, 2nd edn. Springer, New York (2007)
3. Takayama, K., Sasaki, M.: Effects of radius of curvature and initial angle on the shock transition over concave or convex walls. Rep. Inst. High Speed Mech. Tohoku Univ. **46**, 1–30 (1983)
4. Takayama, K., Sekiguchi, H.: An experiment on shock diffraction by cones. Rep. Inst. High Speed Mech. Tohoku Univ. **36**, 53–74 (1977)
5. Yang, M.-J., Sasoh, A., Takayama, K.: The reflection of a shock wave over a cone. Shock Waves **6**, 267–273 (1996)
6. Kuribayashi, T., Ohtani, K., Takayama, K., Menezes, V., Sun, M., Saito, T.: Heat flux measurement over a cone in a shock tube flow. Sock Waves **16**, 275–285 (2007)
7. Watanabe, M., Takayama, K.: Study of reflected shock wave transition over a cone with an angle of attack. In: 1993 Japanese Shock Wave Symp. Sendai, pp. 689–692 (1993). This paper is available in ISWI Proceedings Archive 2007, which contains Japanese Shock Wave Symposium since 1989 offered by ITOCHU Techno Solutions
8. Timofeev, E., Voinovich, P., Saito, T., Takayama, K.: Three-dimensional unsteady reflection of a planar shock wave from an inclined cylinder. In: Proceedings of International Symposium on Interdisciplinary Shock Wave Research, ISISW, Matsushima, Japan, pp. 498–517 (2004). This paper is available in ISWI Proceedings Archive 2007
9. Ohtomo, T., Ohtani, K., Takayama, K.: Attenuation of shock waves propagating over arrayed baffle plate. Shock Waves **14**, 379–390 (2005)
10. Takayama, K., Gotoh, J., Ben-Dor, G.: Influence of surface roughness on the shock wave transition in quasi-stationary and truly non-stationary flows. In: Treanor, C.E., Hall, J.G. (eds.) Shock Tubes and Waves, Proceedings of 13th International Symposium on Shock Tubes and Waves, pp. 326–334 (1981)
11. Meguro, T., Takayama, K., Onodera, O.: Three-dimensional shock wave reflection over a corner of two intersecting wedges. Shock Waves **7**, 107–121 (1997)
12. Henderson, L.F., Takayama, K., Crutchfield, W.Y., Itabashi, S.: The persistence of regular reflection during strong shock diffraction over rigid ramps. J. Fluid Mech. **431**, 273–296 (2001)
13. Smith, L.G.: Photographic investigation of the reflection of plane shocks in air. Off. Sci.Res. Dev. OSSRD Rep 6271, Washington, DC (1945)
14. Takayama, K., Ben-Dor, G., Gotoh, J.: Regular to Mach reflection transition in truly non-stationary flows—influence of surface roughness. AIAA J. **19**, 1238–1240 (1981)
15. Reichenbach, H.: Contributions of Ernst Mach to fluid mechanics. Ann. Rev. Fluid Mech. **15**, 1–29 (1983)